JOURNAL OF GEOPHYSICAL RESEARCH, VOL. 113, G03034, doi:10.1029/2007JG000603, 2008

Combined Simple Biosphere/Carnegie-Ames-Stanford Approach terrestrial carbon cycle model

Kevin Schaefer,[1] G. James Collatz,[2] Pieter Tans,[3] A. Scott Denning,[4] Ian Baker,[4] Joe Berry,[5] Lara Prihodko,[4] Neil Suits,[6] and Andrew Philpott[7]

Received 25 September 2007; revised 15 May 2008; accepted 16 June 2008; published 9 September 2008.

[1] Biogeochemical models must include a broad variety of biological and physical processes to test our understanding of the terrestrial carbon cycle and to predict ecosystem biomass and carbon fluxes. We combine the photosynthesis and biophysical calculations in the Simple Biosphere model, Version 2.5 (SiB2.5) with the biogeochemistry from the Carnegie-Ames-Stanford Approach (CASA) model to create SiBCASA, a hybrid capable of estimating terrestrial carbon fluxes and biomass from diurnal to decadal timescales. We add dynamic allocation of Gross Primary Productivity to the growth and maintenance of leaves, roots, and wood and explicit calculation of autotrophic respiration. We prescribe leaf biomass using Leaf Area Index (LAI) derived from remotely sensed Normalized Difference Vegetation Index. Simulated carbon fluxes and biomass are consistent with observations at selected eddy covariance flux towers in the AmeriFlux network. Major sources of error include the steady state assumption for initial pool sizes, the input weather data, and biases in the LAI.

Citation: Schaefer, K., G. J. Collatz, P. Tans, A. S. Denning, I. Baker, J. Berry, L. Prihodko, N. Suits, and A. Philpott (2008), Combined Simple Biosphere/Carnegie-Ames-Stanford Approach terrestrial carbon cycle model, *J. Geophys. Res.*, *113*, G03034, doi:10.1029/2007JG000603.

1. Introduction

[2] We must understand the biogeochemical processes underlying the terrestrial carbon cycle to evaluate ecosystem function, explain variability in atmospheric composition, and predict future conditions. Models used in atmospheric circulation models or data assimilation require a highly mechanistic terrestrial ecosystem model representing a broad variety of biological and physical processes on timescales of minutes to decades and spatial scales of ~1 km to global. To assimilate observed Net Ecosystem Exchange (NEE), biomass, and atmospheric CO_2 concentrations, the model must accurately represent terrestrial carbon stocks and fluxes. The model must allow for easy addition of new processes without extensive redesign to study the effects of biomass burning, disturbances, and harvesting on carbon stocks and NEE.

[3] NEE is the net CO_2 flux from the terrestrial biosphere:

$$NEE = R_H + R_A - GPP, \quad (1)$$

where R_H is heterotrophic respiration, R_A is autotrophic respiration, and GPP is gross primary production. GPP is the uptake of CO_2 from the atmosphere by plant photosynthesis, R_H is the release of CO_2 due to the decay of organic material by microorganisms, and R_A is the release of CO_2 by plants during maintenance and growth. A positive NEE indicates a net CO_2 flux into the atmosphere. Other than a few tower and aircraft observations, direct measurements of NEE are not possible, so we depend heavily on ecosystem models to provide insight into the carbon cycle. Ecosystem models range from highly mechanistic, process-based models to highly simplified statistical regression models, depending on their intended application.

[4] We combine two existing models, the Simple Biosphere model, version 2.5 (SiB2.5) [*Sellers et al.*, 1996a, 1996b] and the Carnegie-Ames-Stanford Approach (CASA) model [*Potter et al.*, 1993; *Randerson et al.*, 1996], to produce SiBCASA. Both models are fully mature with a long history in a broad variety of research applications. SiB2.5 is a biophysical model estimating surface fluxes of NEE, latent heat, sensible heat, radiant energy, and momentum at high time resolution for use in atmospheric circulation models. Estimating latent heat flux in SiB2.5 requires a mechanistic representation of stomatal conductance, and thus GPP [*Ball*, 1988; *Collatz et al.*, 1991]. CASA is a biogeochemical model with a process-based representation of R_H from a number of distinct organic pools, simulating

[1] National Snow and Ice Data Center, University of Colorado, Boulder, Colorado, USA.
[2] NASA Goddard Space Flight Center, Greenbelt, Maryland, USA.
[3] Earth System Research Laboratory, National Oceanic and Atmospheric Administration, Boulder, Colorado, USA.
[4] Department of Atmospheric Science, Colorado State University, Fort Collins, Colorado, USA.
[5] Department of Global Ecology, Carnegie Institution of Washington, Stanford, California, USA.
[6] Department of Biological and Physical Sciences, Montana State University, Billings, Montana, USA.
[7] Middle Atlantic River Forecast Center, National Weather Service, State College, Pennsylvania, USA.

0148-0227/08/2007JG000603$09.00

long-term changes in terrestrial carbon stocks at daily to monthly time steps.

[5] Neither model alone can meet our needs: SiB2.5 cannot predict biomass, CASA cannot predict NEE on diurnal timescales, and neither can predict R_A. SiB2.5 assumes long-term carbon balance ($NEE = 0$ or $GPP = R_A + R_H$) [*Denning et al.*, 1996], which works well at diurnal to annual timescales, but cannot predict long-term carbon sources and sinks. CASA uses a simple light use efficiency model to estimate Net Primary Productivity ($NPP = GPP - R_A$). This assumes R_A is a constant fraction of *GPP*, but *GPP* occurs only during the day and R_A is continuous, so CASA cannot predict *NEE* on diurnal timescales. SiB2.5 can calculate total respiration ($R_A + R_H$) and CASA NPP, but neither can explicitly estimate R_A. Combining the sophisticated biophysics and *GPP* model from SiB2.5 with the R_H model from CASA produces a hybrid suitable for use in a variety of retrospective analyses and data assimilation focusing on how disturbances, climate, and other factors affect carbon cycle dynamics.

[6] Here we describe SiBCASA and evaluate its performance by comparing modeled and observed NEE and biomass at selected eddy covariance flux towers representing several forest types. We focus on new capabilities not found in either SiB2.5 or CASA and not already described in the peer reviewed literature, emphasizing the dynamics of leaf, root, and wood growth. The auxiliary material[1] contains additional model evaluation, lists the values and references for all biophysical parameters used in SiBCASA, and summarizes the sensitivity of model output to parameter values and initial conditions. Parameter values are chosen based on literature reviews of field observations, independent of the observed NEE and biomass used for model evaluation.

2. SiBCASA Description

[7] To create dynamic controls on GPP allocation, we extensively modified CASA's prognostic equations for the leaf, root, and wood pools. We specified leaf biomass using remotely sensed Leaf Area Index (LAI). We added a storage pool representing available starch for plant growth to explicitly calculate R_A and estimate NEE at the SiB2.5 time step of 10–20 min. The CASA surface litter and soil carbon pools are unchanged, but now use prognostic soil temperature and moisture from SiB2.5 for various scaling factors. We did not modify the SiB2.5 biophysical calculations and GPP model.

2.1. SiB2.5

[8] SiB2.5 is a land-surface parameterization computing surface fluxes at 10–20 min time steps for climate models [*Sellers et al.*, 1986, 1996a, 1996b; *Denning et al.*, 1996]. SiB2.5 has integrated water, energy, and carbon cycles and predicts as prognostic variables the moisture contents and temperatures of the canopy and soil [*Sellers et al.*, 1996a]. *Vidale and Stöckli* [2005] recently added canopy air space CO_2 concentration, humidity, and temperature as prognostic variables. SiB2.5 uses the Community Land Model (CLM) soil model [*Bonan*, 1996] with 10 layers to a depth of 3.3 m. SiB2.5 uses the CLM snow model [*Dai et al.*, 2003], which has a variable number of layers, depending on snowfall amount and history. Fluxes of latent and sensible heat include the effects of snow cover, rainfall interception by the canopy, and aerodynamic turbulence [*Sellers et al.*, 1996a].

[9] To calculate GPP, SiB2.5 uses the Ball-Berry stomatal conductance model [*Ball*, 1988] as modified by *Collatz et al.* [1991] coupled to a modified version of the *Farquhar et al.* [1980] C_3 enzyme kinetic model and the *Collatz et al.* [1992] C_4 photosynthesis model. The semiempirical Ball-Berry model relates stomatal conductance to GPP, linking the exchange of CO_2 and water vapor between the leaf and the canopy air space:

$$g_c = m\frac{A_n}{C_s}h_s P + bLAI \tag{2}$$

where g_c is canopy stomatal conductance, m is an empirical slope from observations, c_s is the CO_2 partial pressure at the leaf surface, h_s is the relative humidity at the leaf surface, P is atmospheric pressure, and b is the minimum possible g_c. A_n is canopy net assimilation:

$$A_n = GPP - R_c, \tag{3}$$

where R_c is the canopy autotrophic respiration to maintain the leaf enzyme infrastructure for photosynthesis. The modified *Farquhar et al.* [1980] enzyme kinetic model assumes the most limiting resource (nitrogen, short wave energy, or leaf export capacity) determines GPP [*Sellers et al.*, 1996a, 1996b]:

$$GPP = Min(W_C, W_E, W_S) \tag{4}$$

where W_C is the Rubisco (leaf enzyme or nitrogen) limited rate, W_E is light limited rate, and W_S for C_3 plants is carbon compound export limited rate. For C_4 plants, W_S is the PEP-Carboxylase limited rate. Both models respond to changing temperature, humidity, and other environmental conditions as described by *Sellers et al.* [1996a, 1996b]. SiB2.5 calculates GPP by iterating the CO_2 partial pressure inside the leaf chloroplasts to minimize the difference between the Ball-Berry and modified *Farquhar et al.* [1980] enzyme kinetic models. GPP and g_c are first calculated for a single leaf at the canopy top and scaled to the entire canopy using absorbed fraction of Photosynthetically Active Radiation (f_{PAR}) derived from Normalized Difference Vegetation Index (NDVI) [*Sellers et al.*, 1994, 1996a, 1996b].

2.2. CASA

[10] CASA represents the flow of carbon between biogeochemical pools as a system of first-order, linear differential equations [*Potter et al.*, 1993]. The carbon in the ith pool (C_i) in a system of n pools varies with time (t) depending on gains from other pools (G_i), transfers to other pools (T_i), respiration loses (R_i), and disturbances (δ_i):

$$\frac{dC_i}{dt} = G_i - T_i - R_i + \delta_i. \tag{5}$$

[1] Auxiliary materials are available in the HTML. doi:10.1029/2007JG000603.

Table 1. SiBCASA Pools

Pool Name	Description
storage	nonstructural carbohydrates
leaf	leaf biomass
root	fine root biomass
wood	woody biomass
CWD	coarse woody debris
surfmet	surface metabolic
surfstr	surface structural
surfmic	surface microbial
soilmet	soil metabolic
soilstr	soil structural
soilmic	soil microbial
slow	soil slow
arm	soil armored

δ_i is the input or removal of carbon by harvest, biomass burning, and other disturbances. G_i depends on transfers from other pools and T_i and R_i depend on C_i:

$$\frac{dC_i}{dt} = \sum_{j=1}^{n} f_{j2i} k_{Tj} C_j - k_{Ti} C_i - k_{Ri} C_i + \delta_i, \tag{6}$$

where k_{Ti} and k_{Ri} are decay rate constants for pool transfers and respiration, and f_{j2i} is the fraction of carbon lost from pool j transferred to pool i. T_i and R_i are typically related, so we define an effective decay rate constant ($k_i = k_{Ti} + k_{Ri}$) and transfer efficiency (e_{j2i}) such that

$$\frac{dC_i}{dt} = \sum_{j=1}^{n} f_{j2i} e_{j2i} k_j C_j - k_i C_i + \delta_i. \tag{7}$$

e_{j2i} is the ratio of carbon received by pool i to carbon lost from pool j, with the rest released as respiration. The respiration from the ith pool is

$$R_i = \sum_{j=1}^{n} \left(1 - e_{i2j}\right) f_{i2j} k_i C_i. \tag{8}$$

[11] The effective decay rate constant varies with environmental conditions, which we represent using scaling factors:

$$k_i = \frac{f_i S_T S_F S_M}{\tau_i}, \tag{9}$$

where τ_i is a reference turnover time, f_i is the available pool fraction, and S_T, S_F, and S_M are temperature, freezing, and moisture scaling factors. τ_i represents an average residence time for carbon in each pool, f_i accounts for partial availability of the pool, and S_T, S_F, and S_M vary from pool to pool.

[12] SiBCASA represents the pool equations in matrix form:

$$\frac{d}{dt}\mathbf{C} = \mathbf{TKC} - \mathbf{KC} + \mathbf{D}, \tag{10}$$

where $\mathbf{C}$ is a vector of n pool sizes, $\mathbf{T}$ is an nxn matrix of transfer fractions and efficiencies, $\mathbf{K}$ is a diagonal, nxn matrix of decay rate constants, and $\mathbf{D}$ is a vector of n disturbance inputs or removals. Only nonzero values of f_{j2i} determine which pools transfer carbon to other pools, so $\mathbf{T}$ represents the pool "configuration" by defining the "flow" of carbon between pools. Because τ_i for the pools are always significantly longer than the SiBCASA 10-min time step, we chose a forward time differencing scheme without risk of numerical instability:

$$\mathbf{C}_{t+\Delta t} = \mathbf{C}_t + \Delta t(\mathbf{TKC}_t - \mathbf{KC}_t + \mathbf{D}), \tag{11}$$

where $\mathbf{C}_t$ are the current pool sizes, $\mathbf{C}_{t+\Delta t}$ are pool sizes for the next time step, and Δt is the SiBCASA time step. The matrix formulation simplifies changing the pool configuration, since all that is required is specifying constants in $\mathbf{T}$ and $\mathbf{K}$.

[13] Table 1 lists the 13 carbon pools in SiBCASA. The storage pool contains Nonstructural Carbohydrates (NC) or starch in the stems and roots used as raw material for plant growth and maintenance. The leaf pool contains leafy biomass and the root pool contains fine root biomass. The wood pool includes above ground wood biomass, woody root tissue, and seeds. The CWD pool consists of dead trees and woody roots. The surface and soil structural pools contain lignin and the metabolic pools contain more labile substrates. The surface and soil microbial pools represent microbial populations. The slow soil pool consists of humus and other recalcitrant organic material. The armored soil pool is organic material bound to clay, which isolates it from microbial decay.

[14] Figure 1 illustrates the flow of carbon between pools, as represented in the $\mathbf{T}$ matrix, with carbon generally flowing from upper left to lower right. Vertical lines represent carbon losses from each pool and horizontal arrows indicate carbon gains to each pool. Dots indicate transfers from one pool to another ($f_{i2j} \neq 0$). For example, carbon lost from the leaf pool is transferred to the surfstr and surfmet pools. The primary input into this system of pools is A_n. Photosynthesis puts starch into the storage pool, while growth and maintenance of leaves, roots, and wood extract starch from the storage pool. As live biomass dies, the lignin fraction is transferred to the structural pools and everything else to the metabolic pools. Microbes consume the most labile material first, processing biomass into the more recalcitrant slow and armored pools. Each time biomass moves from one pool to another, some carbon is lost as respiration.

2.2.1. Surface and Soil Pools

[15] The prognostic equations for the CWD, surface litter, and soil pools are the same as in CASA [*Potter et al.*, 1993], except that SiBCASA uses the SiB2.5 temperature and moisture scaling factors (S_T and S_M) with a new freezing scaling factor (S_F). The CWD and surface pools use the topsoil layer temperature and moisture. For soil pools, we assume the carbon per layer is proportional to observed root density profiles, which decrease exponentially, with nearly all roots (and thus soil carbon) within the top 1 m of soil. We calculate k_i, the nonzero entries in the $\mathbf{K}$ matrix, as a root fraction weighted average of S_T, S_F, and S_M from each soil layer:

$$k_i = \frac{f_i}{\tau_i} \sum_{k=1}^{m} f_{rootk} S_{Tk} S_{Fk} S_{Mk}, \tag{12}$$

where m is the number of soil layers, S_{Tk}, S_{Fk}, and S_{Mk} are soil temperature, freezing, and moisture scaling factors, and

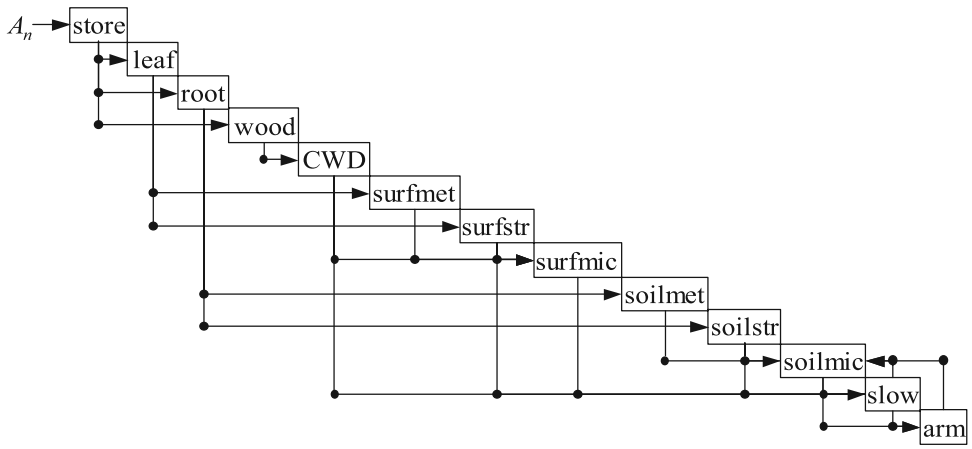

Figure 1. The SiBCASA pool configuration, with carbon flowing from upper left to lower right. Vertical lines represent pool losses, horizontal arrows represent pool gains, and dots represent transfers between pools. The primary input is canopy net assimilation (A_n) into the storage pool.

f_{rootk} are the fraction of total roots in soil layer k. f_{rootk} are time invariant based on average, biome dependant root density profiles [*Jackson et al.*, 1996].

[16] Microbial activity, and thus R_H, increases with soil temperature such that

$$S_T = Q_{10}^{\frac{(T-T_{ref})}{10}}, \tag{13}$$

where, T is soil temperature, T_{ref} is a reference temperature, and Q_{10} is the factor by which respiration changes for a 10 K change from T_{ref} [*Raich and Schlesinger*, 1992; *Denning et al.*, 1996; *Potter et al.*, 1993]. S_T overestimates R_H in frozen soil, so S_F inhibits microbial activity below freezing using a curve fit to incubated soil samples [*Mikan et al.*, 2002]:

$$S_F = \frac{1}{1+\exp(T_{half}-T)}, \tag{14}$$

where T_{half}(K) is the half-point temperature. The presence of minute clay particles act to depress the freezing point of water, limiting microbial activity in frozen soil to thin water films coating soil grains. As temperatures drop below freezing, the water films become thinner and microbial activity rapidly decreases, effectively ceasing below temperatures of -7 to -8°C [*Oechel et al.*, 1997; *Mast et al.*, 1998; *Hobbie et al.*, 2000; *Mikan et al.*, 2002]. R_H peaks when the soil volume is about 15% air: too much water limits microbial oxygen supply while too little water limits microbial population. S_M scales R_H relative to the optimal value using a curve fit to laboratory observations of incubated soil samples [*Raich et al.*, 1991; *Denning et al.*, 1996]:

$$S_M = 0.2 + R_{sat}^B, \tag{15}$$

where B is the wetness exponent,

$$B = \left(\frac{W^{skew} - W_{opt}^{skew}}{1 - W_{opt}^{skew}}\right)^2, \tag{16}$$

and W is soil moisture fraction of saturation, W_{opt} is the optimal saturation fraction, *Skew* is the skewness exponent, and R_{sat} determines R_H at saturation.

2.2.2. Leaf and Root Pools

[17] Leaf biomass is prescribed using remotely sensed LAI and we assume root growth is proportional to leaf growth. We linearly interpolate between monthly NDVI composite values to determine an instantaneous LAI growth rate (ΔLAI). Positive ΔLAI represents new leaf growth and negative ΔLAI represents dead leaves transferred to surface litter pools. For forest biomes, leaf pool gain (G_{leaf}) includes new leaf growth and replacement of dead evergreen leaves:

$$G_{leaf} = LMA_{eff}\left(\Delta LAI + k_{leaf} LAI_{\min}\right), \tag{17}$$

where LMA_{eff} is the canopy effective leaf mass per leaf area, k_{leaf} is the evergreen leaf decay constant, and $LAI_{\min}$ is the long-term, minimum LAI. NDVI specifies growth of perennial leaves, so k_{leaf} applies only to the evergreen portion of total LAI, which we assume is $LAI_{\min}$.

[18] For grasslands, we include the transition between C_3 and C_4 herbaceous plants. Since LAI represents a grid cell average, we assume f_{CA}, the fractional area coverage of C_4 plants, also represents the C_4 fraction of LAI:

$$G_{leaf} = LMA_{eff}\left(\Delta LAI + k_{leaf} LAI + \Delta f_{C4} LAI\right), \tag{18}$$

where Δf_{C4} is the rate of change in area coverage fraction of C_4 grasses. In some extra-tropical systems, C_3 grasses and forbs dominate in the spring and early summer while C_4 grasses dominate in the late summer and fall. During transitions between C_3 and C_4 cover, old leaves die and new leaves grow, even though LAI may remain nearly constant. Δf_{C4} is interpolated from monthly values in the same manner as ΔLAI. Monthly values of f_{C4} come from field observations at some sites.

[19] LMA_{eff} accounts for the fact that sunlit leaves have a greater mass per area than shaded leaves. Leaf mass varies linearly with visible light intensity, peaking at the canopy top and decreasing to approximately half the maximum value at the canopy bottom [*Aranda et al.*, 2004]. We assume leaf growth and senescence is evenly distributed

throughout the canopy. Using Beer's law to represent the relative intensity of visible light and integrating through the canopy according to *Sellers et al.* [1996b] gives:

$$LMA_{eff} = LMA_{top} r_{sunshade} \left(1 + \frac{f_{PAR\max} - f_{PAR}}{f_{PAR\max} - f_{PAR\min}}\right), \quad (19)$$

where LMA_{top} is the leaf mass per area at the canopy top, $r_{sunshade}$ is the ratio of sun to shade leaf mass, and f_{PAR}max and f_{PAR}min are the theoretical maximum and minimum values of f_{PAR}. f_{PAR} saturates as LAI increases, so LMA_{eff} approaches a constant value representing a weighted average between sunlit and shaded leaves.

[20] We assume k_{leaf} varies only with canopy temperature:

$$k_{leaf} = \frac{S_{Tleaf}}{\tau_{leaf}}, \quad (20)$$

where S_{Tleaf} is a temperature scaling factor and τ_{leaf} is evergreen leaf lifetime. For S_{Tleaf} we apply the SiB2.5 temperature scaling function for R_c [*Sellers et al.*, 1996a]:

$$S_{Tleaf} = \frac{2.0^{(T_{can} - T_{ref})/10}}{1 + \exp(S_{RD}(T_{can} - T_{RD}))}, \quad (21)$$

where T_{can} is the prognostic canopy temperature, T_{ref} is a reference temperature, S_{RD} is the inhibition slope and T_{RD} is the half point temperature.

[21] We assume fine root growth is proportional to leaf growth, so $G_{root} = S_{rootshoot} G_{leaf}$, where G_{root} is root growth and $S_{rootshoot}$ is the root-to-shoot ratio (the ratio of below to above ground biomass, excluding wood). Fine root growth is controlled by both environmental factors and plant phenology, but is closely synchronized to leaf growth such that the root to shoot ratio stays fairly constant with time [*Gaucher et al.*, 2005]. In SiBCASA, root growth is specified by NDVI, but root mortality is not, so

$$\frac{dC_{root}}{dt} = S_{rootshoot} G_{leaf} - k_{root} C_{root} + \delta_{root}, \quad (22)$$

where k_{root} is a root mortality decay rate constant. We assume k_{root} does not vary in time (S_T, S_F, and S_M all equal one).

2.2.3. Storage Pool

[22] The storage pool, C_{store}, consists of NC or soluble sugars and starch [*Piispanen and Saranpaa*, 2001; *Barbaroux and Breda*, 2002; *Gaucher et al.*, 2005]. A_n adds NC to the storage pool, while growth and maintenance of leaves, roots, and wood extract NC from the storage pool:

$$\frac{dC_{store}}{dt} = A_n - L_{leaf} - L_{root} - L_{wood}, \quad (23)$$

where L_{leaf}, L_{root}, and L_{wood} are NC losses to the leaf, root, and wood pools. The SiB2.5 half of SiBCASA calculates A_n as part of the GPP calculations [*Sellers et al.*, 1996a]. Leaf and root growth are specified from LAI, so $L_{leaf} = G_{leaf}/e_{store2leaf}$ and $L_{root} = S_{rootshoot} G_{leaf}/e_{store2root}$, where $e_{store2leaf}$ and $e_{store2root}$ are NC to leaf and root conversion efficiencies. We assume wood growth depends on available NC, so $L_{wood} = k_{store} C_{store}$, where k_{store} is the storage pool decay rate constant. Seasonally varying controls on k_{store} represent the effects of environmental conditions on wood growth:

$$k_{store} = \frac{f_{sugar} S_{density} S_{Tstore} S_{Fstore} S_{Mstore}}{\tau_{store}}, \quad (24)$$

where f_{sugar} is the sugar fraction of NC, $S_{density}$ is the ratio of earlywood to latewood density, and S_{Tstore}, S_{Fstore}, and S_{Mstore} are temperature, frost, and moisture scaling factors.

[23] We assume that the environmental controls for wood growth are the same as those for photosynthesis, so we apply the formulations for S_{Tstore}, S_{Fstore}, and S_{Mstore} from the SiB2.5 photosynthesis model to wood growth. S_{Tstore} inhibits wood growth when the canopy temperature is either too hot or too cold [*Sellers et al.*, 1996a]:

$$S_{Tstore} = \frac{1}{\left(1 + \exp\left(S_L\left(T_{Lhalf} - T_{can}\right)\right)\right)\left(1 + \exp\left(S_H\left(T_{can} - T_{Hhalf}\right)\right)\right)}, \quad (25)$$

where S_L and S_H are the slopes of low and high temperature inhibition functions, and T_{Lhalf} and T_{Hhalf} are half point temperatures. S_{Fstore} represents the effects of frost by stopping wood growth for temperatures near or below freezing:

$$S_{Fstore} = \frac{1}{\left(1 + \exp\left(S_F\left(T_{Fhalf} - T_{min}\right)\right)\right)}, \quad (26)$$

where S_F is the slope and T_{Fhalf} the half point of the frost inhibition function, and $T_{\min}$ is a running minimum canopy temperature. Plants take time to recover from the effects of frost, which we model by increasing $T_{\min}$ by 2°C per day. If T_{can} is less than $T_{\min}$, $T_{\min}$ is reset to T_{can} and frost recovery resumes. Wood growth stops when the soil is too dry [*Bouriaud et al.*, 2004], so S_{Mstore} represents the effect of drought stress on wood growth:

$$S_{Mstore} = \frac{(1.0 + p) f_{PAW}}{(p + f_{PAW})}, \quad (27)$$

where f_{PAW} is the plant available water fraction and p is the stress shape parameter. f_{PAW} is the total column liquid water above the wilting point divided by the total possible available water based on soil field capacity. p determines the plant sensitivity to drought stress between field capacity and wilting point with an assumed value of 0.2.

[24] f_{sugar} accounts for the fact that only the sugar portion of the storage pool is available for wood growth. In woody plants, most NC is starch while sugar, primarily sucrose, is the principle raw material for wood growth [*Piispanen and Saranpaa*, 2001]. Trees biochemically convert starch into sugar and back as needed, with f_{sugar} varying between 5 and 30%, depending on species and time of year [*Piispanen and Saranpaa*, 2001; *Barbaroux and Breda*, 2002; *Gaucher et al.*, 2005]. We assume f_{sugar} is 0.1 for all biome types based on observed NC in oak trees [*Barbaroux and Breda*, 2002].

Table 2. Flux Tower Sites for Model Evaluation

Tower Name	Biome	Location	References
Harvard Forest (main tower)	Deciduous Needleleaf Forest	Harvard Forest, MA USA	*Barford et al.* [2001]
Howland Forest (main tower)	Deciduous Needleleaf Forest	Howland Forest, ME, USA	*Hollinger et al.* [2004]
WLEF tall tower	Deciduous Needleleaf Forest	Park Falls, WI, USA	*Berger et al.* [2001]; *Davis et al.* [2003]
BOREAS Old Black Spruce	Needleleaf Forest	Manitoba, Canada	*Dunn et al.* [2007]
Santarem	Tropical Forest	Santarem (Km67), Brazil	*Saleska et al.* [2003]

[25] $S_{density}$ accounts for seasonal changes in wood density. Earlywood forms in spring during leaf growth while latewood forms after leaf growth stops. Earlywood is less dense than latewood because it contains more vessels for water and nutrient transport to the leaves. Since radial growth rate is constant throughout the growing season [*Barbaroux and Breda*, 2002], wood growth is less in spring than in summer. In spring, $S_{density}$ equals the ratio of earlywood to latewood density. In summer, after leaf growth has stopped, $S_{density}$ equals one.

2.2.4. Wood Pool

[26] The wood pool, C_{wood}, depends on wood growth, tree mortality, and sapwood maintenance:

$$\frac{dC_{wood}}{dt} = e_{store2wood} k_{store} C_{store} - k_{wood} C_{wood} - \frac{f_{sapwood} S_{Tstore}}{\tau_{sapwood}} C_{wood}, \tag{28}$$

where $e_{store2wood}$ is the NC to wood conversion efficiency, k_{wood} is the tree mortality decay rate constant, $f_{sapwood}$ is the sapwood fraction of the wood pool, and $\tau_{sapwood}$ is the sapwood turnover time. The center of a stem consists of heartwood that contains no living cells. Sapwood between the cambium and heartwood conducts water and nutrients to the leaves and contains a small fraction of live, radial parenchyma cells that store NC. Maintenance of parenchyma cells varies with temperature [*Edwards and Hanson*, 1996], so we apply the same temperature scaling factor that modulates wood growth, S_{Tstore}. We assume a constant value of $\tau_{sapwood}$ for all biome types based on observed sapwood respiration rates per volume of wood. We use a constant, average $f_{sapwood}$ based on observations from multiple tree species.

3. Model Evaluation

3.1. Observations

[27] We evaluate SiBCASA by comparing simulated and observed NEE and biomass at five eddy covariance flux towers representing a range of forest types (Table 2). All the forest tower sites have estimates of wood biomass based on biometric measurements. Observed NEE is the covariance between vertical wind speed and CO_2 concentration averaged over 30-min time intervals [*Baldocchi*, 2003]. Although eddy covariance techniques cannot distinguish between GPP and total ecosystem respiration ($R_T = R_H + R_A$), one can estimate GPP by statistically training a respiration model using nighttime and winter NEE and temperature data, and subtracting the results from daytime NEE. Separate estimates of R_T and GPP are available at Boreas, Harvard, and Santarem. To quantify SiBCASA performance, we calculate a residual between monthly averages of simulated and observed NEE:

$$\delta = NEE_{obs} - NEE_{SiBCASA}. \tag{29}$$

The mean residual, δ_{mean}, represents the bias between observed and simulated NEE. The residual standard deviation, δ_{std}, measures the match between simulated and observed variability.

3.2. Simulation Setup

[28] We estimate f_{PAR}, LAI, and vegetation cover fraction from the GIMMS NDVI data set, version g [*Tucker et al.*, 2005] using procedures described by *Sellers et al.* [1996b], *Los et al.* [2001], and *Schaefer et al.* [2002, 2005]. GIMMS consists of global, monthly composite maps of NDVI at 8 km resolution adjusted for missing data, satellite orbit drift, differing instrument calibrations, sensor degradation, and volcanic aerosols. We extract NDVI for each tower location and assign a SiBCASA biome type that most closely matches the local vegetation. We assign biome specific biophysical parameters from *Sellers et al.* [1996b]. If available, we use observed soil texture at each tower site. If not, we use soil textures from $1^\circ \times 1^\circ$ maps of percent sand, silt, and clay interpolated from the International Global Biosphere Program soil core database.

[29] As input weather, we extract data for each tower from the NCEP reanalysis [*Kalnay et al.*, 1996] interpolated to $1^\circ \times 1^\circ$ resolution. Observations at each tower include local weather conditions, but SiBCASA requires continuous data and filling the inevitable gaps in observed weather is difficult and time consuming. The NCEP reanalysis contains surface temperature, pressure, wind speed, precipitation, and radiation data every six hours from 1958 to 2003. Except for incident light, SiBCASA linearly interpolates NCEP weather in time between input data points. We scale incident light by the cosine of the solar zenith angle to conserve incoming energy and assure no light falls on the canopy at night [*Zhang et al.*, 1996].

[30] We assume steady state conditions for initial pool sizes, which implies mature ecosystems with no disturbances where growth balances decay and NEE ~ 0. The steady state assumption is typical for many biogeochemical models because observations of biomass and detrital pools often do not exist. The armored pool, with $\tau \sim 222$ years, may require 5000 or more simulation years to achieve steady state. Such long simulations are impractical with SiBCASA's 10-min time step, so we set time derivatives in the pool equations to zero and algebraically solve for steady state pool sizes:

$$0 = [\bar{\mathbf{T}}\bar{\mathbf{K}} - \bar{\mathbf{K}}]\mathbf{C}_{steady} + \bar{\mathbf{D}}, \tag{30}$$

where $\mathbf{C}_{steady}$ is a vector of steady state pool sizes and the overbars represent long-term means. In $\bar{\mathbf{T}}$, only the transfer fractions from storage to the leaf, root, and wood pools vary with time. We don't include disturbances in these test

Table 3. SiBCASA Performance at Flux Tower Sites

Tower Name	δ_{mean} (μmol m^{-2} s^{-1})	δ_{std} (μmol m^{-2} s^{-1})
Harvard Forest	−0.75	2.00
Howland Forest	−1.12	1.09
WLEF tall tower	−0.11	0.76
BOREAS	−0.07	1.02
Santarem	−0.86	2.83

simulations, so $\bar{\mathbf{D}}$ only includes the time mean A_n into the storage pool. We adjust $\mathbf{C}_{steady}$ to match the amplitude and phasing of each pool's average seasonal cycle. We run three simulations at each tower: the first estimates $\mathbf{C}_{steady}$, the second balances *NEE* within 1%, and the third balances *NEE* within 0.5%. The earliest flux data starts in 1991 and the 1° × 1° NCEP reanalysis ended in 2003, so all simulations started in 1990 and ended in 2003.

[31] In some simulations we use the "quasi-steady state" assumption to initialize the pools using observed wood biomass. We set initial wood biomass equal to an observed value and assume the other pools are in equilibrium with wood. The wood pool is by far the largest carbon pool at all the forest sites and is the dominant source of detrital matter to the soil and surface pools. Quasi-steady state assumes the faster CWD, surface, and soil pools reach equilibrium relative to the wood pool long before the wood pool itself reaches equilibrium.

[32] At Harvard, Howland, Boreas, and WLEF, we also compare simulated and observed biomass as a function of stand age from disturbance. Following *Masek and Collatz* [2006], we assume each site is logged and remove 90% of the above ground wood. Assuming 75% of wood is above ground [*Jenkins et al.*, 2001], we transfer 22.5% of the wood to the CWD pool, and the rest is removed. We assume 80% mortality in the fine root pool and transfer the dead fine roots to the soil structural and metabolic pools. To estimate wood carbon from observed aboveground biomass, we assume 50% of wood is carbon [*Miller et al.*, 2004] and 75% is above ground [*Jenkins et al.*, 2001]. We ran 200 year simulations at each site by repeating the 1990–2003 NCEP weather and NDVI.

4. Results

[33] Table 3 summarizes SiBCASA performance. Negative δ_{mean} indicate the average observed NEE is less than the simulated NEE. At steady state, the simulated NEE $\sim$ 0, so all these sites indicate net carbon sinks of various magnitudes. Below we explore why SiBCASA performs better at some sites than others and, when possible, identify techniques to improve performance.

4.1. Mixed Deciduous Forest

[34] Harvard Forest, Howland Forest, and WLEF are deciduous or mixed deciduous/evergreen forests of varying stand age. The match between simulated and observed NEE improves with increasing stand age as the steady state assumption becomes more applicable (Figures 2–4). SiBCASA shows the best match at WLEF, which has a stand age of 60–80 years and is near steady state [*Davis et al.*, 2003]. Howland (90–140 year stand age) and Harvard (60 year stand age) have stronger sinks indicative of younger, less mature stands [*Barford et al.*, 2001; *Hollinger et al.*, 2004].

[35] Differences in biomass between and young and mature forests can partly explain differences between modeled and observed fluxes at the three mixed forest sites. Younger stands not in steady state have less dead biomass and lower R_H, resulting in larger summer drawdown and a stronger overall sink. The match between simulated and observed NEE improves if we use the quasi-steady state assumption and observed wood biomass. The WLEF and Howland simulations show only slight changes because they are closer to steady state (not shown). The improvement is

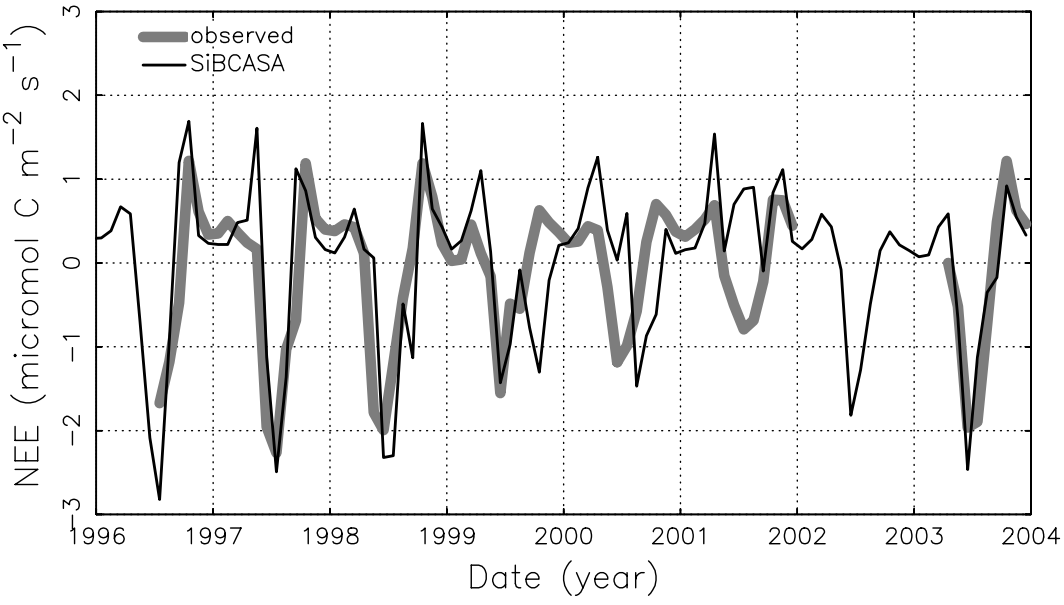

Figure 2. Observed (gray) and simulated (black) NEE at WLEF.

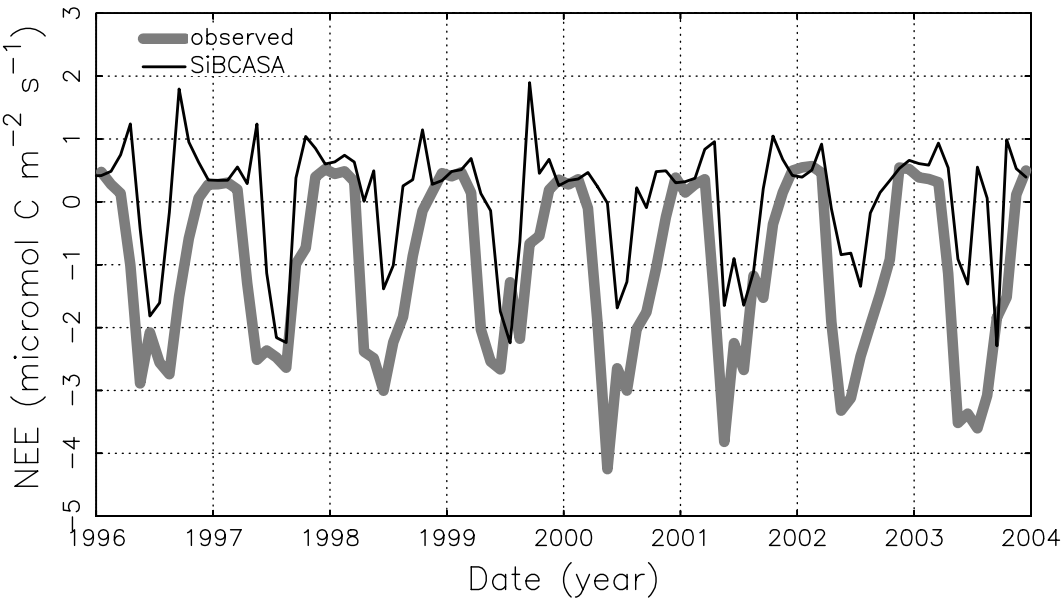

Figure 3. Observed (gray) and simulated (black) NEE at Howland Forest.

greatest at Harvard, which has the youngest stand age and is not near steady state (Figure 4).

[36] At Harvard Forest, the quasi-steady state assumption only decreases δ_{mean} to 0.57 because observed wood biomass improves simulated summer NEE drawdown, but makes the winter NEE worse. At steady state, the simulated R_T is nearly double observed R_T, but at quasi-steady state, simulated R_T closely matches observed R_T (see auxiliary material). However, SiBCASA overestimates GPP in winter because the NCEP reanalysis is warmer in winter than observed (see auxiliary material). The pixel containing Harvard Forest in the original 1.875° × 1.904° NCEP data is partly ocean, resulting in a less extreme diurnal variation in temperature. Interpolating to 1° × 1° does not change the diurnal cycle, resulting in warmer than observed temperatures and GPP in winter. Using gap-filled observed weather [*Stöckli et al.*, 2008] improves the match between simulated and estimated GPP (see auxiliary material).

[37] The simulated storage pool is consistent with observations of total NC in various deciduous trees (Figure 5). NC as a function of time is measured by taking tree ring cores at regular time intervals, drying them, and using chemical washes to extract soluble starches and sugars. Observations are expressed as mg NC per g of dry wood, so dividing the storage pool by the wood pool allows a reasonable comparison with field data. Lacking NC observations at the tower sites, we compare our modeled NC with available observations for sessile oak and European beech in France for 1998 [*Barbaroux and Breda*, 2002], yellow birch and sugar maple in southeast Canada in 1998

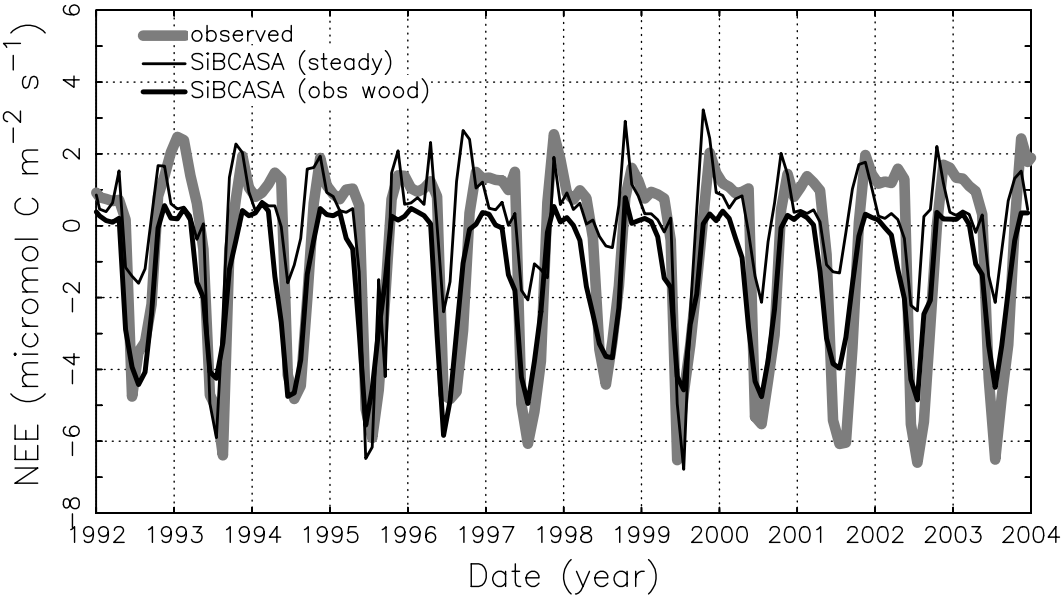

Figure 4. Observed NEE (gray), simulated NEE assuming steady state (thin black), and simulated NEE with observed wood biomass (thick black) at Harvard Forest.

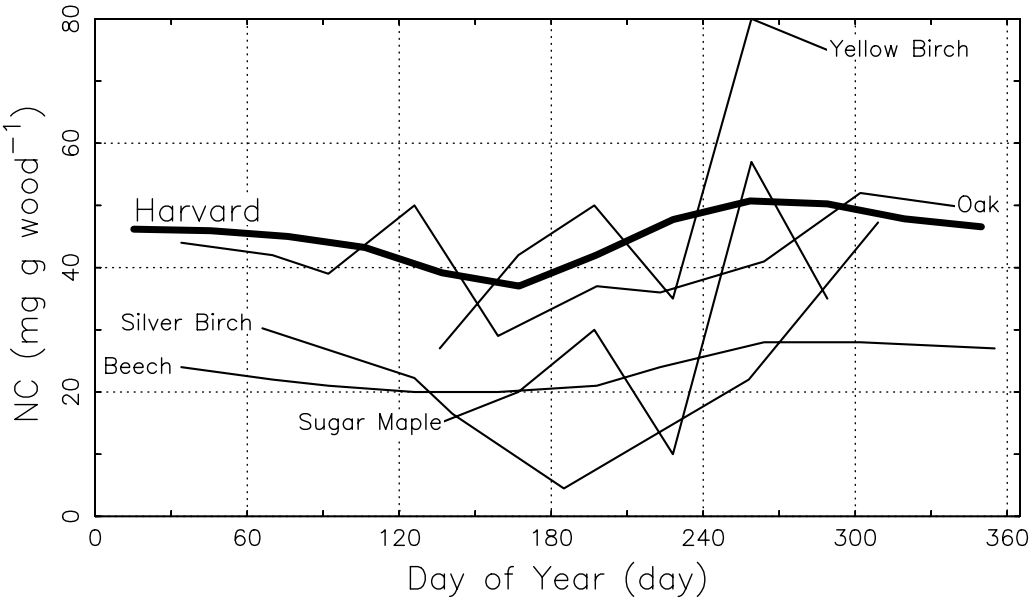

Figure 5. Observed NC for various hardwood species (thin lines) and the average seasonal cycle of simulated NC at Harvard Forest (thick line).

[*Gaucher et al.*, 2005], and silver birch in Finland in 1996–7 [*Piispanen and Saranpaa*, 2001]. The average simulated seasonal cycle at Harvard best matches the beech observations in amplitude and timing, but the magnitude best matches the oak observations. Howland and WLEF show similar seasonal cycles with average values at 54 ± 7 and 45 ± 11mg NC per g of dry wood respectively (not shown). The simulated NC at all three sites are well within the ±20–50% tree-to-tree and interannual variability in observed NC.

4.2. Boreal Forest

[38] At the Boreas Old Black Spruce site modeled and observed fluxes do not match very well due to a snow cover bias in the estimated LAI (Figure 6). This site consists of needleleaf, evergreen trees with an understory dominated by mosses [*Dunn et al.*, 2007]. Accounting for perennial plants and deciduous brush, we expect to see some seasonal variation in LAI, but the LAI algorithm misinterprets the burial of vegetation by snow as an annual loss of leaves. The peak summer LAI of ~4 m^2 m^{-2} matches observed values [*Gower et al.*, 2001], but the seasonal variation of 3.8 m^2 m^{-2} is unrealistic. Regrowing all leaves each year produces large, physically unrealistic spikes in R_A and R_H and greatly reduces the available NC, resulting in significantly less simulated wood than observed. The Boreas site is fully mature with a stand age of ~120 years, so the

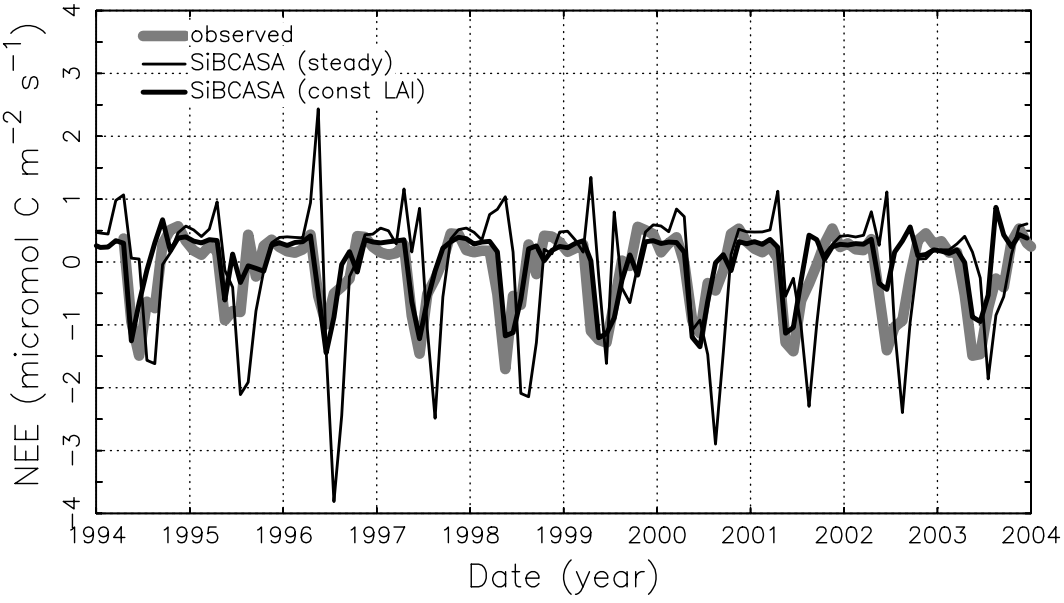

Figure 6. Observed NEE (gray), simulated NEE with variable LAI (thin black), and simulated NEE with constant LAI (thick black) at BOREAS old black spruce.

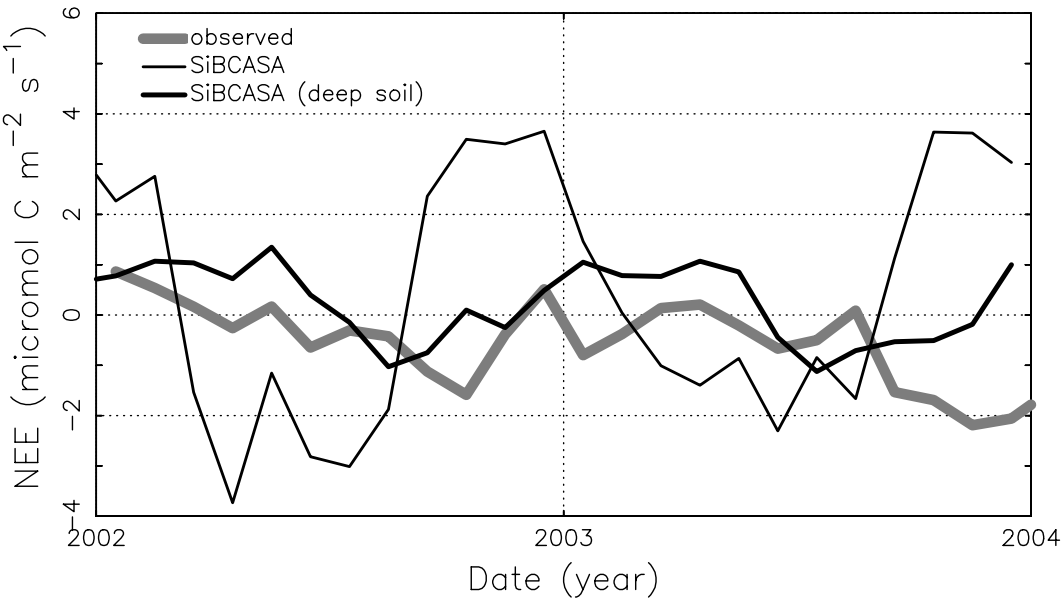

Figure 7. Observed NEE (gray), simulated NEE with variable LAI and a shallow soil depth (thin black), and simulated NEE with constant LAI and a deep soil layer (thick black) at Santarem (km 67).

steady state assumption applies. The observed wood biomass is ~71 Mg C ha^{-1} [*Gower et al.*, 2001] while the simulated wood with snow biased LAI is ~47 Mg C ha^{-1}.

[39] Assuming constant LAI equal to the maximum value produces much more realistic simulated NEE (Figure 6). With or without assuming constant LAI, the simulated GPP about 10–15% higher than observed (see auxiliary material). Since Boreas is in steady state, the simulated R_T is also 10–15% higher than observed (see auxiliary material). The excess GPP in combination with constant LAI results in simulated wood biomass that is too large (~112 Mg C ha^{-1}). We can partly attribute this to the fact that the observed precipitation is less than the NCEP precipitation, resulting in less simulated drought stress in summer than observed. However, we did not have gap-filled observed weather data to test how strongly using observed precipitation affects the simulated fluxes and biomass.

4.3. Tropical Forest

[40] At Santarem (km67), a tropical evergreen forest in the Amazon Basin, simulated biomass is consistent with observed, but SiBCASA produces a strong seasonal cycle in simulated NEE that is out of phase with observations (Figure 7). The site is near steady state with simulated wood biomass of 256 Mg C ha^{-1}, consistent with observed wood biomass of 246–273 Mg C ha^{-1} based on three separate biometric surveys [*Miller et al.*, 2004]. The simulated seasonal cycles of R_T and GPP are much stronger than observed (see auxiliary material), resulting in a NEE seasonal cycle in NEE much stronger than observed.

[41] The differences between observed and simulated fluxes result from noisy NDVI and excessive modeled drought stress in SiBCASA. Clouds, water vapor, and aerosols contaminate the NDVI, resulting in an unrealistic 50% reduction in LAI at Santarem during the rainy season and producing a fairly strong seasonal cycle in simulated R_T from the decay and regrowth of leaves. The trees at Santarem have deep tap roots which, when combined with hydraulic redistribution by roots [*Lee et al.*, 2005], provide sufficient water for photosynthesis in the dry season [*Saleska et al.*, 2003]. However, the soil in SiBCASA extends only to ~3.3 m depth, which is not deep enough to represent deep water access by tap roots, resulting in seasonally varying GPP due to excessive simulated drought stress.

[42] Eliminating NDVI noise by assuming a constant LAI equal to the maximum observed value removes the seasonality in simulated R_T, but not the seasonality in simulated GPP. GPP depends on f_{PAR}, which is much less sensitive to noise and tends to saturate to a maximum value of ~0.95 for LAI > 2 m^2 m^{-2}. With LAI peaking at ~7 m^2 m^{-2}, even a 50% seasonal cycle in LAI does not significantly change f_{PAR} to affect GPP.

[43] Increasing the total depth of the soil column from 3.3 m to 15 m greatly increases the water available for plant growth, eliminating the simulated drought stress and resulting in a nearly constant GPP. This, in combination with constant LAI, significantly improves the match between the simulated and observed NEE, reducing δ_{std} to 0.88 μmol m^{-2} s^{-1} (Figure 7), but simulated GPP, R_T, and wood biomass are all ~20% higher than observed. Using observed, gap-filled weather [*Stöckli et al.*, 2008] in combination with constant LAI and a deep soil column does not effect NEE, but results in simulated GPP and R_T that match estimated values quite well (see auxiliary material). Similar experiments at the nearby logged site produce similar results (not shown).

4.4. Stand Age Experiments

[44] Simulated wood biomass as a function of stand age is consistent with observed values derived from biometric measurements. Figure 8 shows simulated and observed wood biomass as a function of stand age at Harvard, Howland, Boreas, and WLEF [*Curtis et al.*, 2002; *Hollinger et al.*, 2004]. Figure 8 also shows average observed wood biomass in the northeast U.S. from the national Forest

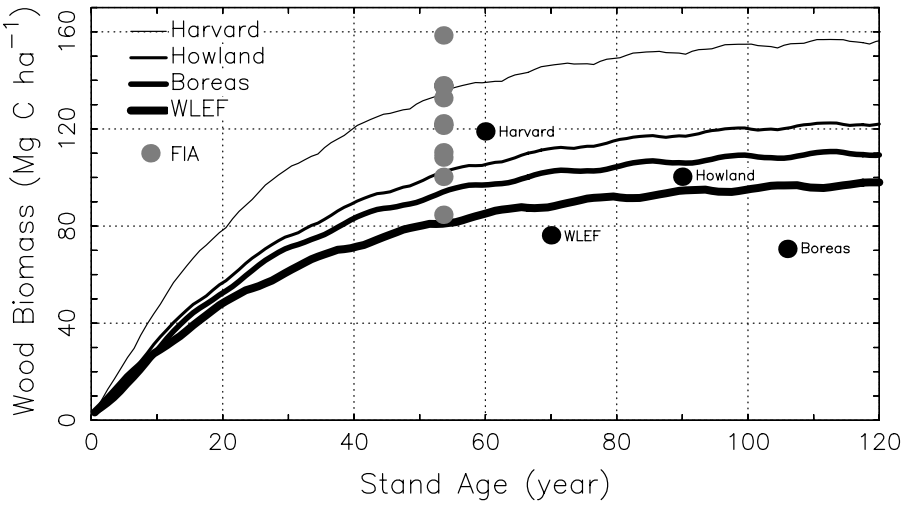

Figure 8. Simulated and observed wood biomass at Harvard, Howland, Boreas, and WLEF as a function of stand age. Lines are simulated values; labeled dots are locally observed values; gray dots are values from the Forest Inventory Analysis (FIA).

Inventory Analysis (FIA) at an average stand age of 53.6 ± 22.4 years [*Jenkins et al.*, 2001]. Simulated wood biomass approaches steady state between 100 and 150 years after the initial disturbance, depending on site. Repeating the same 14 years of NCEP weather replicates the pattern of inter-annual variability, giving the simulated wood biomass curves a distinctive wavy look.

[45] At all four sites, simulated wood biomass falls within the spread of observed wood biomass from the FIA sites, but is slightly higher than locally observed. We can attribute part of this small, positive bias to differences between observed and NCEP weather increasing GPP, as seen at Harvard Forest. However, part of the bias also results from the fact that our wood pool includes seeds. Seed growth can consume between 3 and 20% of annual GPP, depending on species. A separate seed pool would have a turnover of ~1 year, but when combined with the wood pool, seed biomass has an effective turnover equivalent to wood, resulting in a positive bias. Even with this positive bias, however, the simulated wood biomass at all four sites fall within the 30% uncertainty in biometric-based biomass estimates [*Jenkins et al.*, 2001].

[46] Extending these 200-year simulations out to 5000 years validated our algebraic calculation of steady state pool sizes. Within 10–15 years after the initial disturbance, the litter and soil pools reached steady state relative to the wood pool, confirming our quasi-steady state calculations. After 100–150 years, the wood, litter and soil pools all reached their long-term steady state values. The armored pool, with its 222-year turnover time, took 3000–5000 years to reach steady state. The difference in flux between the 200-year and 5000-year simulations was minor since respiration from the armored pool at most accounted for only 0.5% of R_H.

5. Discussion

[47] SiBCASA's simulated biomass and seasonal variability of NEE are generally consistent with observations at flux towers in the AmeriFlux network. When run to stand age after disturbance, simulated wood biomass at all forest sites is slightly higher than observed, but still within the uncertainty of the biometric measurements. The seasonal cycle and magnitude of simulated NC for deciduous and mixed deciduous-evergreen forests are well within the variability of available observations. We found three main sources of mismatch between simulated and observed fluxes and biomass: initial pool sizes (particularly wood), input weather, and biases in the LAI.

[48] The steady state assumption for initial pool sizes works well for mature forests sites, but not for young forests, which are not in steady state. Initializing pools with observed wood using the quasi-steady state assumption improves the simulated fluxes, but observed wood biomass is typically unavailable. Spinning up to stand age from a disturbance also improves the simulated fluxes, but is computationally expensive and observed stand age is also often unavailable.

[49] We can partially attribute differences between observed and simulated NEE to errors in the input weather from the NCEP reanalysis data. Although useful, reanalysis products have significant deficiencies, especially with precipitation [*Costa and Foley*, 1998; *Betts et al.*, 2005]. Higher precipitation than observed resulted in increased GPP at Boreas. Higher than observed temperatures at night at Harvard resulted in excessive simulated GPP in winter. Using observed weather improves the simulation results, as we saw at Harvard Forest, but observed weather is not available at all sites and not available globally.

[50] Using LAI from NDVI to specify leaf biomass has advantages and disadvantages. NDVI products are readily available, global in coverage, well understood, and widely used. Using NDVI to drive the seasonal cycle of NEE in a global atmospheric circulation model produces a better match with observed CO_2 concentration than prognostic vegetation models [*Heimann et al.*, 1998]. NDVI offers observational constraints on leaf growth, but does not provide the ability to predict into the future. Currently available NDVI data sets contain biases and noise that result in false variability in LAI. LAI is sensitive to small changes in NDVI, so errors in NDVI cause SiBCASA to incorrectly lose and regrow leaves,

producing unrealistic spikes in R_T, drawing too much carbon from the storage pool, and stunting wood growth.

[51] Nearly all sites showed some problems with the LAI, but by far Santarem, with cloud and aerosol contamination, and Boreas, with snow cover bias, had the largest NDVI errors. NDVI errors fall into three categories: atmospheric contamination, snow cover, and temporal interpolation; all of which produce false variability in LAI. At Santarem, the LAI signal contains considerable noise consistent with cloud, water vapor, and aerosol contamination, fluctuating up and down as much as 4.0 m^2 m^{-2} in a single month. Simulated GPP, which depends on f_{PAR}, is much less sensitive to NDVI errors, so false variability in NDVI does not often produce obvious problems in simulated GPP. At Boreas, for example, the snow cover bias mimics the effects of seasonal variation in temperature on GPP. Interpolating between monthly composite values does not capture the rapid changes in LAI during spring and fall. Using 15-day rather than monthly NDVI composites can better resolve seasonal transitions, but are noisier, worsening problems associated with false LAI variability.

[52] These problems with NDVI are not new, but linking simulated leaf biomass directly to NDVI now requires a better treatment of snow cover, cloud, aerosol, and water vapor contamination when estimating LAI. Developing practical techniques to minimize atmospheric contamination and counter the effects of snow cover is a difficult and ongoing task. Improved interpolation techniques, better representation of plant phenology, longer compositing periods, and enhanced radiative transfer models with snow cover, clouds, and aerosols can improve the estimation of LAI from NDVI.

6. Conclusions

[53] We successfully integrated the biogeochemical model CASA into the biophysical model SiB2.5 to produce the hybrid SiBCASA. Simulated biomass and carbon flux are consistent with observations at flux towers in the AmeriFlux network. Major sources of uncertainty include the initial pool sizes (particulary wood biomass), input weather, and biases in the LAI.

[54] SiBCASA can simulate long-term carbon sources and sinks, which SiB2.5 could not. A new NC storage pool, not present in CASA, allows SiBCASA to stockpile starch for use when needed. In addition to using f_{PAR} derived NDVI to drive GPP, SiBCASA also uses LAI derived from NDVI to prescribe leaf and root growth. This, in combination with the new storage pool and wood growth controls, allows dynamic allocation of GPP to leaf, root, and wood growth, instead of fixed fractions of annual GPP as seen in CASA. The storage pool and dynamic allocation also allow explicit estimation of R_A, absent in both SiB2.5 and CASA. The new matrix pool formulation simplifies changing the pool configuration and adding disturbance processes. The simple procedure to initialize the pools assuming steady state or quasi-steady state with observed wood greatly reduces spinup time.

[55] SiBCASA is suitable for a variety of research applications to study processes affecting the carbon cycle. The biophysical processes from SiB and the biogeochemical processes from CASA combined with high time resolution and short spinup time make SiBCASA well suited for use in global or regional atmospheric circulation models. The biogeochemistry from CASA fully integrated with the photosynthesis from SiB2.5 make SiBCASA suitable for data assimilation of a variety of trace gas, flux, and biomass observations. Prognostic biomass combined with a simple matrix pool design simplifies the representation of various disturbances, such as biomass burning and harvest. SiBCASA can be run "off-line" with reanalysis products and observed, gap-filled weather for a variety of process-based studies relating climate to the carbon cycle. The quasi-steady state assumption allows initialization of pools using gridded maps of observed wood biomass derived from forest inventory data, which will greatly improve estimates of regional or global carbon fluxes.

[56] **Acknowledgments.** This research was funded by the National Research Council Research Associateship Program in collaboration with Colorado State University under National Aeronautics and Space Administration (NASA) grant NNG05GD15G, NASA grant NNX06AE65G, NASA subcontract NNG05GF41G, National Oceanic and Atmospheric Administration grant NA07OAR4310115, and the Carbon Science Group at the NASA Goddard Space Flight Center. We thank the AmeriFlux Principle Investigators for providing the flux observations used in this study: P. Bakwin, B. Cook, K. Davis, M. Goulden, D. Hollinger, T. Meyers, R. Teclaw, S. Verma, W. Wang, K. Wilson, S. Wofsy, and C. Yi.

References

Aranda, I., F. Pardo, L. Gil, and J. A. Pardos (2004), Anatomical basis of the change in leaf mass per area and nitrogen investment with relative irradiance within the canopy of eight temperate tree species, *Acta Oecologica-Intl, J. Ecol.*, *25*(3), 187–195.

Baldocchi, D. D. (2003), Assessing the eddy covariance technique for evaluating carbon dioxide exchange rates of ecosystems: Past, present and future, *Global Change Biol.*, *9*(4), 479–492, doi:10.1046/j.1365-2486.2003.00629.x.

Ball, J. T. (1988), An analysis of stomatal conductance, Ph.D. thesis, Stanford Univ., Stanford, Calif.

Barbaroux, C., and N. Breda (2002), Contrasting distribution and seasonal dynamics of carbohydrate reserves in stem wood of adult ring-porous sessile oak and diffuse-porous beech trees, *Tree Physiol.*, *22*, 1201–1210.

Barford, C. C., S. C. Wofsy, M. L. Goulden, J. W. Munger, E. H. Pyle, S. P. Urbanski, L. Hutyra, S. R. Saleska, D. Fitzjarrald, and K. Moore (2001), Factors controlling long- and short-term sequestration of atmospheric CO_2 in a mid-latitude forest, *Science*, *294*(5547), 1688–1691, doi:10.1126/science.1062962.

Berger, B. W., K. J. Davis, C. X. Yi, P. S. Bakwin, and C. L. Zhao (2001), Long-term carbon dioxide fluxes from a very tall tower in a northern forest: Flux measurement methodology, *J. Atmos. Oceanic Technol.*, *18*(4), 529–542, doi:10.1175/1520-0426(2001)018<0529:LTCDFF>2.0.CO;2.

Betts, A. K., J. H. Ball, P. Viterbo, A. Dai, and J. Marengo (2005), Hydrometeorology of the Amazon Basin, *J. Hydrometeorol.*, *6*, 764–774, doi:10.1175/JHM441.1.

Bonan, G. B. (1996), A Land Surface Model (LSM Version 1.0) for ecological, hydrological, and atmospheric studies: Technical description and users guide, *NCAR Tech. Note NCAR/TN-417+STR*, Natl. Cent. for Atmos. Res., Boulder, Colo.

Bouriaud, O., N. Breda, G. Le Moguedec, and G. Nepveu (2004), Modeling variability of wood density in beech as affected by ring age, radial growth, and climate, *Trees (Berl.)*, *18*, 264–276, doi:10.1007/s00468-003-0303-x.

Collatz, G. J., J. T. Ball, C. Grivet, and J. A. Berry (1991), Physiological and environmental regulation of stomatal conductance, photosynthesis, and transpiration: A model that includes a laminar boundary layer, *Agric. For. Meteorol.*, *54*, 107–136, doi:10.1016/0168-1923(91)90002-8.

Collatz, G. J., M. Ribascarbo, and J. A. Berry (1992), Coupled photosynthesis-stomatal conductance model for leaves of C_4 plants, *Aust. J. Plant Physiol.*, *19*(5), 519–538.

Costa, M. H., and J. A. Foley (1998), A comparison of precipitation datasets for the Amazon Basin, *Geophys. Res. Lett.*, *25*(2), 155–158, doi:10.1029/97GL03502.

Curtis, P. S., P. J. Hanson, P. Bolstad, C. Barford, J. C. Randolph, H. P. Schmid, and K. B. Wilson (2002), Biometric and eddy-covariance based estimates of annual carbon storage in five eastern North American deciduous forests, *Agric. For. Meteorol.*, *113*(1–4), 3–19, doi:10.1016/S0168-1923(02)00099-0.

Dai, Y., et al. (2003), The common land model, *Bull. Am. Meteorol. Soc.*, *84*(8), 1013–1023, doi:10.1175/BAMS-84-8-1013.

Davis, K. J., P. S. Bakwin, C. X. Yi, B. W. Berger, C. L. Zhao, R. M. Teclaw, and J. G. Isebrands (2003), The annual cycles of CO_2 and H_2O exchange over a northern mixed forest as observed from a very tall tower, *Global Change Biol.*, *9*(9), 1278–1293, doi:10.1046/j.1365-2486.2003.00672.x.

Denning, A. S., G. J. Collatz, C. Zhang, D. A. Randall, J. A. Berry, P. J. Sellers, G. D. Colello, and D. A. Dazlich (1996), Simulations of terrestrial carbon metabolism and atmospheric CO_2 in a general circulation model, Part 1: Surface carbon fluxes, *Tellus*, *48*, 521–542, doi:10.1034/j.1600-0889.1996.t01-2-00009.x.

Dunn, A. L., C. C. Barford, S. C. Wofsy, M. L. Goulden, and B. C. Daube (2007), A long-term record of carbon exchange in a boreal black spruce forest: Means, responses to interannual variability, and decadal trends, *Global Change Biol.*, *13*(3), 577, doi:10.1111/j.1365-2486.2006.01221.x.

Edwards, N. T., and P. J. Hanson (1996), Stem respiration in a closed-canopy upland oak forest, *Tree Physiol.*, *16*(4), 433–439.

Farquhar, G. D., S. von Caemmerer, and J. A. Berry (1980), A biochemical model of photosynthetic CO_2 assimilation in leaves of C_3 species, *Planta*, *149*, 78–90, doi:10.1007/BF00386231.

Gaucher, C., S. Gougeon, Y. Mauffette, and C. Messier (2005), Seasonal variation in biomass and carbohydrate partitioning of understory sugar maple (Acer saccharum) and yellow birch (Betula alleghanienis) seedlings, *Tree Physiol.*, *25*, 93–100.

Gower, S. T., O. Krankina, R. J. Olson, M. Apps, S. Linder, and C. Wang (2001), Net primary production and carbon allocation patterns of boreal forest ecosystems, *Ecol. Appl.*, *11*(5), 1395–1411, doi:10.1890/1051-0761(2001)011[1395:NPPACA]2.0.CO;2.

Heimann, M., et al. (1998), Evaluation of terrestrial carbon cycle models through simulations of the seasonal cycle of atmospheric CO_2: First results of a model intercomparison study, *Global Biogeochem. Cycles*, *12*(1), 1–24, doi:10.1029/97GB01936.

Hobbie, S. E., J. P. Schimel, S. E. Trumbore, and J. R. Randerson (2000), Controls over carbon storage and turnover in high-latitude soils, *Global Change Biol.*, *6*, 196–210, suppl. 1.

Hollinger, D. Y., et al. (2004), Spatial and temporal variability in forest-atmosphere CO_2 exchange, *Global Change Biol.*, *10*(11), 1961–1961, doi:10.1111/j.1365-2486.2004.00892.x.

Jackson, R. B., J. Canadell, J. R. Ehleringer, H. A. Mooney, O. E. Sala, and E. D. Schulze (1996), A global analysis of root distributions for terrestrial biomes, *Oecologia*, *108*, 389–411, doi:10.1007/BF00333714.

Jenkins, J. C., R. A. Birdsey, and Y. Pan (2001), Biomass and NPP estimation for the mid-Atlantic region (USA) using plot-level forest inventory data, *Ecol. Appl.*, *11*(4), 1174–1193, doi:10.1890/1051-0761(2001)011[1174:BANEFT]2.0.CO;2.

Kalnay, E., et al. (1996), The NCEP/NCAR 40-year reanalysis project, *Bull. Am. Meteorol. Soc.*, *77*(3), 437–471, doi:10.1175/1520-0477(1996)077<0437:TNYRP>2.0.CO;2.

Lee, J. E., R. S. Oliveira, T. E. Dawson, and I. Fung (2005), Root functioning modifies seasonal climate, *Proc. Natl. Acad. Sci. U. S. A.*, *102*, 17,576–17,581, doi:10.1073/pnas.0508785102.

Los, S. O., G. J. Collatz, L. Bounoua, P. J. Sellers, and C. J. Tucker (2001), Global interannual variations in sea surface temperature and land-surface vegetation, air temperature, and precipitation, *J. Clim.*, *14*(7), 1535–1549, doi:10.1175/1520-0442(2001)014<1535:GIVISS>2.0.CO;2.

Masek, J. G., and G. J. Collatz (2006), Estimating forest carbon fluxes in a disturbed southeastern landscape: Integration of remote sensing, forest inventory, and biogeochemical modeling, *J. Geophys. Res.*, *111*, G01006, doi:10.1029/2005JG000062.

Mast, M. A., K. P. Wickland, R. T. Striegl, and D. W. Clow (1998), Winter fluxes of CO_2 and CH_4 from subalpine soils in Rocky Mountain National Park, Colorado, *Global Biogeochem. Cycles*, *12*(4), 607–620, doi:10.1029/98GB02313.

Mikan, C. J., J. P. Schimel, and A. P. Doyle (2002), Temperature controls of microbial respiration in arctic tundra soils above and below freezing, *Soil Biol. Biochem.*, *34*(11), 1785–1795, doi:10.1016/S0038-0717(02)00168-2.

Miller, S. D., M. L. Goulden, M. C. Menton, H. R. da Rocha, H. C. de Freitas, A. M. E. S. Figueira, and C. A. D. de Sousa (2004), Biometric and micrometeorological measurements of tropical forest carbon balance, *Ecol. Appl.*, *14*(4), S114–S126, suppl. S, doi:10.1890/02-6005.

Oechel, W. C., G. Vourlitis, and S. J. Hastings (1997), Cold season CO_2 emission from arctic soils, *Global Biogeochem. Cycles*, *11*(2), 163–172, doi:10.1029/96GB03035.

Piispanen, R., and P. Saranpaa (2001), Variation of non-structural carbohydrates in silver birch (Betula pendula Roth) wood, *Trees (Berl.)*, *15*, 444–451, doi:10.1007/s004680100125.

Potter, C. S., J. T. Randerson, C. B. Field, P. A. Matson, P. M. Vitousek, H. A. Mooney, and S. A. Klooster (1993), Terrestrial ecosystem production: A process-oriented model based on global satellite and surface data, *Global Biogeochem. Cycles*, *7*, 811–842, doi:10.1029/93GB02725.

Raich, J. W., and W. H. Schlesinger (1992), The global carbon dioxide flux in soil respiration and its relationship to vegetation and climate, *Tellus, Ser. B*, *44*, 81–99, doi:10.1034/j.1600-0889.1992.t01-1-00001.x.

Raich, J. W., E. B. Rastetter, J. M. Melillo, D. W. Kicklighter, P. A. Steudler, and B. J. Peterson (1991), Potential net primary prodution in South America: Application of a global model, *Ecol. Appl.*, *1*(4), 399–429, doi:10.2307/1941899.

Randerson, J. T., M. V. Thompson, T. J. Conway, C. B. Field, and I. Y. Fung (1996), Substrate limitations for heterotrophs: Implications for models that estimate the seasonal cycle of atmospheric CO_2, *Global Biogeochem. Cycles*, *10*(4), 585–602, doi:10.1029/96GB01981.

Saleska, S. R., et al. (2003), Carbon in Amazon forests: Unexpected seasonal fluxes and disturbance-induced losses, *Science*, *302*(5650), 1554–1557, doi:10.1126/science.1091165.

Schaefer, K., A. S. Denning, N. Suits, J. Kaduk, I. Baker, S. Los, and L. Prihodko (2002), Effect of climate on interannual variability of terrestrial CO_2 fluxes, *Global Biogeochem. Cycles*, *16*(4), 1102, doi:10.1029/2002GB001928.

Schaefer, K., A. S. Denning, and O. Leonard (2005), The winter Arctic Oscillation, the timing of spring, and carbon fluxes in the Northern Hemisphere, *Global Biogeochem. Cycles*, *19*, GB3017, doi:10.1029/2004GB002336.

Sellers, P. J., Y. Mintz, Y. C. Sud, and A. Dalcher (1986), A Simple Biosphere model (SiB) for use within general circulation models, *J. Atmos. Sci.*, *43*(6), 505–531, doi:10.1175/1520-0469(1986)043<0505:ASBMFU>2.0.CO;2.

Sellers, P. J., C. J. Tucker, G. J. Collatz, S. O. Los, C. O. Justice, D. A. Dazlich, and D. A. Randall (1994), A global 1° by 1° NDVI data set for climate studies, part II: The generation of global fields of terrestrial biophysical parameters from NDVI, *Int. J. Remote Sens.*, *15*(17), 3519–3545, doi:10.1080/01431169408954343.

Sellers, P. J., D. A. Randall, G. J. Collatz, J. A. Berry, C. B. Field, D. A. Dazlich, C. Zhang, G. D. Collelo, and L. Bounoua (1996a), A revised land surface parameterization of GCMs, Part I: Model formulation, *J. Clim.*, *9*(4), 676–705, doi:10.1175/1520-0442(1996)009<0676:ARLSPF>2.0.CO;2.

Sellers, P. J., S. O. Los, C. J. Tucker, C. O. Justice, D. A. Dazlich, G. J. Collatz, and D. A. Randall (1996b), A revised land surface parameterization of GCMs, Part II: The generation of global fields of terrestrial biophysical parameters from satellite data, *J. Clim.*, *9*(4), 706–737, doi:10.1175/1520-0442(1996)009<0706:ARLSPF>2.0.CO;2.

Stöckli, R., D. M. Lawrence, G.-Y. Niu, K. W. Oleson, P. E. Thornton, Z.-L. Yang, G. B. Bonan, A. S. Denning, and S. W. Running (2008), Use of FLUXNET in the community land model development, *J. Geophys. Res.*, *113*, G01025, doi:10.1029/2007JG000562.

Tucker, C. J., J. E. Pinzon, M. E. Brown, D. A. Slayback, E. W. Pak, R. Mahoney, E. F. Vermote, and N. El Saleous (2005), An extended AVHRR 8-km NDVI dataset compatible with MODIS and SPOT vegetation NDVI data, *Int. J. Remote Sens.*, *26*(20), 4485–4498, doi:10.1080/01431160500168686.

Vidale, P. L., and R. Stöckli (2005), Prognostic canopy air space solutions for land surface exchanges, *Theor. Appl. Climatol.*, *80*, 245–257, doi:10.1007/s00704-004-0103-2.

Zhang, C., D. A. Dazlich, D. A. Randall, P. J. Sellers, and A. S. Denning (1996), Calculation of the global land surface energy, water, and CO_2 fluxes with an off-line version of SiB2, *J. Geophys. Res.*, *101*(D14), 19,061–19,075, doi:10.1029/96JD01449.

I. Baker, A. S. Denning, and L. Prihodko, Department of Atmospheric Science, Colorado State University, Fort Collins, CO 80523, USA.

J. Berry, Department of Global Ecology, Carnegie Institution of Washington, Stanford, CA 94305, USA.

G. J. Collatz, NASA Goddard Space Flight Center, Greenbelt, MD 20771, USA.

A. Philpott, Middle Atlantic River Forecast Center, National Weather Service, State College, PA 16803, USA.

K. Schaefer, National Snow and Ice Data Center, University of Colorado, Boulder, CO 80309-0449, USA. (kevin.schaefer@nsidc.org)

N. Suits, Department of Biological and Physical Sciences, Montana State University, Billings, MT 59101, USA.

P. Tans, Earth System Research Laboratory, National Oceanic and Atmospheric Administration, Boulder, CO 80305, USA.